BNL-69319
Informal Report

Chemically Bonded Cements from Boiler Ash and Sludge Wastes

Phase I Report
(August 1997- July 1998)

By
Toshifumi Sugama

Energy Efficiency and Conservation Division
Department of Applied Science
Brookhaven National Laboratory
Upton, New York 11973

Kenneth A. Yager

KeySpan Corporation
KeySpan System Laboratory
Shore Road, Glenwood Gas Plant
Glenwood Landing, New York 11547

For
KeySpan Corporation

Project Manager
Mr. Kenneth Black
KeySpan R&D Initiative

August 1998

KEYSPAN

Chemically Bonded Cements from Boiler Ash and Sludge Wastes

Phase I Report
(August 1997- July 1998)

By
Toshifumi Sugama

Energy Efficiency and Conservation Division
Department of Applied Science
Brookhaven National Laboratory
Upton, New York 11973

Kenneth A. Yager

KeySpan Corporation
KeySpan System Laboratory
Shore Road, Glenwood Gas Plant
Glenwood Landing, New York 11547

For
KeySpan Corporation

Project Manager
Mr. Kenneth Black
KeySpan R&D Initiative

August 1998

KEYSPAN

DISCLAIMER

Available electronically at-

`http://www.doe.gov/bridge`

Available to U.S. Department of Energy and its contractors in paper from-

U.S. Department of Energy
Office of Scientific and Technical Information
P.O. Box 62
Oak Ridge, TN 37831
(423) 576-8401

Available to the public from-

U.S. Department of Commerce
National Technical Information Service
5285 Port Royal Road
Springfield, VA 22131
(703) 487-4650

Printed on recycled paper

TABLE OF CONTENTS

	Pages
ABSTRACT	1
1. Introduction	2
2. Theory of CBC	4
3. Experimental Procedures	5
3.1 Materials	5
3.2 Measurements	5
4. Results and Discussion	6
4.1 Chemical Analyses of Wastes	6
4.2 Pb-exchange Adsorbents (PES)	7
4.3 High-performance Cements (HPC)	9
4.3.1 Exothermal Acid-Base Reaction	9
4.3.2 Compressive Strength	11
4.3.3 Phase Identification and Development of Microstructure	12
5. Conclusion	16
References	19

LIST OF TABLES

	Pages
1. XPS surface chemical analysis at BNL for BA and WWTS generated from KeySpan's power stations	20
2. Amounts of total metals existing in the dry BA and WWTS wastes	21
3. Concentrations of metals leached out from the BA and WWTS in accordance with TCLP	21
4. Mix formulations of the KeySpan waste-based cements	22
5. Pb leachability from $Pb(NO_3)_2$-incorporated cements after curing for 1, 7, and 21 days at room temperature	23
6. Pb, V, and Ni leachability of 21-day-aged cements	24
7. Mix formulations of cement slurries	25
8. Exothermal reaction parameters of the 100/0, 90/10, 80/20, 70/30, and 60/40 BA/CAC ratio specimens	26
9. Compressive strength of the specimens with different BA/CAC ratios and the Type I portland cement specimens at early curing times for up to 24 hours	27

LIST OF FIGURES

	Pages
1. Parks's equation for the isoelectric point (IEPS) of particle surfaces	28
2. Waste water treatment sludge (WWTS) from KeySpan's power plants	29
3. Boiler ash (BA) generated from KeySpan's power plants	30
4. Crusher used to convert bulky BA into powders	31
5. Sieve size analysis of crushed BA powders	32
6. XRD pattern of crushed BA powders	33
7. FT-IR spectrum of BA powders	34
8. Non-isothermal DSC curve showing total acid-base exothermal reaction energy	35
9. Compressive strength versus concentration of $-(-NaPO_3-)-_n$	36
10. Changes in compressive strength for the 80°C-autoclaved cement specimens as a function of BA/CAC ratio	37
11.Changes in compressive strength for BA cement and commercial Type I cement specimens as function of curing time in air or water at room temperature	38

LIST OF FIGURES (cont.)

Pages

12. XRD patterns for (a) CAC additive, (b) raw BA powder, (c)28-day-air-cured BA-39$NaPO_3$ system, (d) 80°C steam-cured BA-$NaPO_3$ system, (e) 28-day-air-cured BA-CAC-$NaPO_3$ system, (f) 28-day-water-cured BA-CAC-$NaPO_3$ system, and (g) 80°C-steam-cured BA-CAC-$NaPO_3$ system — 39

13. SEM images for (a) 28-day-air-cured BA-$NaPO_3$ system, (b) 80°C-steam-cured BA-40$NaPO_3$ system, (c) 28-day-air-cured BA-CAC-$NaPO_3$ system, and (d) 28-day-water-cured BA-CAC-$NaPO_3$ system — 40

14. Well-crystallized calcium phosphate phase in 80°C-steam-cured BA-CAC-$NaPO_3$ system — 41

ABSTRACT

In exploring methods to recycle boiler ash (BA) and waste water treatment sludge (WWTS), by-products generated from KeySpan's power plants, into commercially viable materials, we synthesized chemically bonded cements (CBC) offering the following three specific characteristics; 1) immobilization of hazardous heavy metals, such as Pb, Ni, and V, 2) rapid hardening and setting properties, and 3) development of high mechanical strength. The CBCs were prepared through an acid-base reaction between these by-products acting as the solid base reactants and the sodium polyphosphate solution as the cement-forming acid reactant, followed by a hydrating reaction. Furthermore, two additives, the calcium aluminate cements (CAC) and the calcium silicate cements (CSC) were incorporated into the CBC systems to improve their properties. Using a CBC formulation consisting of 53.8 wt% WWTS, 23.1 wt% CSC, and 23.1 wt% [40 wt% -(-$NaPO_3$-)-$_n$], the Toxicity Characteristics Leaching Procedure (TCLP) tests showed that the concentrations of Pb, Ni, and V metals leached out from the specimens were minimal. This formulation originally contained ~ 28800 mg/kg of Pb, ~ 6300 mg/kg of Ni, and ~ 11130 mg/kg of V; the amounts leaching into the acid extraction fluid were only 0.15 mg/L of Pb, 0.15 mg/L of Ni, and 4.63 mg/L of V. On the other hand, CBC specimens derived from a formulation consisting of 42 wt% BA, 18 wt% CAC and 40 wt% [40 wt% -(-$NaPO_3$-)-$_n$] displayed an excellent compressive strength of 10.8 MPa at an early curing age of 2 hours after mixing at room temperature. The reason for its rapid hardening was due to a high exothermic energy evolved by the acid-base reaction. Furthermore, when these specimens were immersed for 28 days in water at 25°C, and exposed for 20 hours to steam at 80°C, a very high compressive strength of > 32 MPa developed. Two physico-chemical factors played an important role in improving the mechanical strength of the specimens: One was the formation of two well-crystallized phases, hydroxyapatite [$Ca_5(PO_4)_3(OH)$] and sodium vanadium sulfate hydrate [$Na_2V(SO_4)_2.4H_2O$], as the reaction products in the cement bodies; the other factor reflected the dense microstructure developed by the growth of these crystalline reaction products.

Accordingly, the CBCs derived from these by-products have a high potential for use as remediating material for hazardous heavy metal-contaminated soils, as rapid-setting repair

patching and filling materials for damaged roadways and bridge decks, and also as binders in precast concrete products, such as blocks, slabs, and pipes.

1. Introduction

According to KeySpan, the annual accumulation of waste water treatment sludge (WWTS, ~ 35 wt% solid sludge) and boiler ash (BA) waste generated in their power plants is projected to be ~ 2400 wet tons and ~ 270 tons in 1999, respectively. These wastes contain heavy metals such as vanadium (V) and nickel (Ni), and must be disposed of in accordance with New York State hazardous waste regulations. The annual cost for their unit collection and disposal was estimated to be ~ $ 200,000. This fact has driven KeySpan to look for ways of recycling these wastes into potentially useful materials, and concurrently reducing the costs associated with their disposal. Also, KeySpan is interested in developing explicit strategies to integrate industrial ecology and green chemistry.

Under the sponsorship of the Office of Geothermal Technologies, U.S. Department of Energy (DOE, Raymond LaSala, project manager), the two-step reaction pathways, acid-base and hydration, for preparing novel chemically bonded cement and ceramic (CBC) materials are being studied at Brookhaven National Laboratory (BNL). These state-of-the-art materials offer many desirable characteristics such as high mechanical strength, low permeability to water, thermal and hydrothermal stability, low rates of carbonation, acid resistance, and good adherence to metal and concrete substrates [1-3]. CBCs are primarily formed by acid-base chemical reactions between two chemical components, the basicity as a proton accepting cation-leachable powder and the acidity as a proton-donating liquid. The powdery solid reactants which serve as fundamental cementitious components include the following six groups: 1) caustic alkalis, MOH; 2) metal oxides, MO; 3) non-silicate salts, MCO_3 and MSO_4; 4) silicates, $M_2O.nSiO_2$; 5) aluminate, $M_2O.nAl_2O_3$; and 6) alunminosilicates, $M_2O.Al_2O_3.(2\text{-}6)SiO_2$. In these formulas, M represents alkali, alkaline earth, and transition metals. The cement-forming acidic reactants are phosphate-based compounds, such as monobasic, MH_2PO_4, dibasic M_2HPO_4, tribasic M_3PO_4, and polybasic $-[-MPO_3-]-_n$; where M is NH_4^+, Na^+, K^+, or Li^+ [4].

For solid reactants, emphasis in the DOE program is being placed on using industrial by-products, such as granulated blast-furnace slags, meta-kaoline, and coal combustion fly ash to establish an industrial recycling system in which these by-product materials are used effectively, not wasted nor allowed to exacerbate environmental impacts and concerns. Some of these by-products contain chemical constituents similar to those in WWTS and BA wastes.

The other environmental issue confronting KeySpan was the contamination of soil brought about by lead (Pb) pigment present in the paint fragments peeled and stripped off from high voltage towers and their facilities. Although only the superficial layers of soil were contaminated, such sites must be cleaned up to eliminate the risk of contaminating the groundwater after long periods, or of exposing children to pollutants in the surface soil. Currently, there are three technologies to remedy polluted sites [5]; 1) hauling the contaminated soil to a landfill and replacing it with clean soil, 2) chemically immobilizing and stabilizing Pb, and 3) leaching out the metals with a soil-washing method using acids. The second technology is of particular interest to us in immobilizing Pb into solid and inert forms. Important factors contributing to the success of this strategy include the requirements that the solid forms have excellent stability and technical performance so that they retain toxic Pb even when exposed to potential leachant solutions.

Based upon this information, the research program at BNL sponsored by KeySpan is aimed at alleviating environmental concerns, reducing the disposal costs of these wastes, and developing process technologies that recycle these wastes of negative value into commercially viable products. The program also seeks potential applications for them, with the economic benefits that may accrue from selling the end-use products. BNL's approach to achieving these goals is to focus on synthesizing and formulating CBC from these WWTS and BA wastes, to assess their abilities to immobilize Pb in contaminated soil, and to use as the binder in building and civil engineering material systems. The first CBC material, called Pb-exchange adsorbent (PEA), is used for dealing with environmental problems as a means of remediating Pb-contaminated soil, and the second one, called high-performance cement (HPC), provides CBC-

based concrete for potential use in KeySpan precast products, such as building blocks and pipes. In addition, both PEA and HPC materials must have the ability to intercalate and encapsulate the V and Ni metals present in the raw WWTS and BA wastes.

2. Theory of CBC

The most important factor affecting the kinetics of the acid-base reaction is the negative charge density of MO lattice (M represents alkali, alkaline earth, and transition metals) which is balanced by cations. When the negative charge density of MO is increased, it becomes increasingly susceptible to penetration by protons. Thus, an MO structure having a high negative charge density is vulnerable to acid attack, thereby disrupting the lattices. Once disruption occurs, a decomposition process will liberate the cations stacked up in the MO lattices. The charge density on the particle's surfaces can be estimated by measuring zeta potential (Z-P), which is the electric potential at the boundary between the particle's surfaces, charged by electrochemical adsorption of atmospheric ions, such as H^+ or OH^-. Since the relative amount of adsorbed H^+ and OH^- ions depends on the pH of the surrounding solution, the pH required to reduce the Z-P to zero charge (equal amounts of adsorbed OH^- or H^+ ions) is the isoelectric point (IEPS) of the particle's surface [6]. Hence, it is possible to rationalize that particle's surfaces with a high and low IEPS reflect the basic and acidic natures, respectively, and a neutral surface has an IEPS of seven [7]. Parks [8] showed that the IEPS for an oxide and hydroxide depends on the valence (Z) and the ionic radius (R) of the cation, as shown in Figure 1.

In synthesizing CBC, attention should be paid to the magnitude of the interfacial acid-base reaction. Its extent can be predicted from an expression derived from Parks's Equation, which refers to the IEPS of the hydrous metal oxide surfaces and the dissociation constants (pK) of cement-forming liquids. This expression is as follows:

$$\Delta A = \text{IEPS} - pK_A \qquad (1),$$

where ΔA is the magnitude of surface interaction of hydrous metal oxides, and pK_A is the acid dissociation constant. Referring to Eq. (1), a higher positive ΔA value is indicative of stronger interfacial bonding. Thus, the magnitude in bond strength of the reaction products of acid with

the basic MO reactants can be theoretically estimated from the IEPS-Z/R relation (see Figure 1). Our unpublished study on reviewing Parks's equation demonstrated that the IEPS of Ca oxide is higher than that of Mg oxide, suggesting that Ca oxide, with the highest IEPS, is the most reactive cation-leachable single oxide component against the acidic reactants (data not shown). As seen in Figure 1 , together with our unpublished work, the oxide compounds with IEPS of > 10 , which can be classified as base reactants having a strong affinity for acid reactants, included the following elementals: Ca, Mg, Fe, Co, Ni, Pb, Cd, La, and Be.

3. Experimental Procedures

3.1 Materials

Two waste materials, WWTS (Figure 2), and BA (Figure 3) acting as base powder reactants, were supplied by KeySpan. The "as-received" WWTS contained free water of ~ 65 wt%. The raw BA was a rock-like hard bulky solid, and was powdered using a crusher (Retrch Type BB1A, Brinkmann, Co., see Figure 4). The distribution of particle size for the crushed BA was given in Figure 5. A granular polybasic sodium phosphate, [-(-$NaPO_3$-)-$_n$, (Aldrich Chemical Company)], known as intermediator of fertilizer, was dissolved in water to make a 10, 20, 30, and 40 wt% -(-$NaPO_3$-)-$_n$ solution, and was used as the acid reactant. Two cement additives, Refcon as calcium aluminate cement (CAC) and Type I as calcium silicate cement (CSC), were obtained from the Lehigh Portland Cement Company. The X-ray diffraction (XRD) analyses showed that the major chemical components of the CAC were composed of monocalcium aluminate, monocalcium dialuminate, and gehlenite; the principal component of CSC was tricalcium silicate. These additives were used to accelerate the acid-base reaction.

3.2 Measurements

The leachability of the hazardous heavy metals such as Pb, Ni, and V, from the solidified binder matrix was detected by the Toxicity Characteristics Leaching Procedure (TCLP) recommended by the U.S. Environmental Protection Agency (EPA). The leachates were analyzed for Pb, Ni, and V ion concentrations using atomic absorption spectrophotometry (AA). A combination of analytical techniques, including x-ray photoelectron spectroscopy (XPS), x-ray

powder diffraction (XRD), energy-dispersive x-ray spectrometry (EDX), and Fourier transform-infrared (FT-IR), were used to inspect the chemical constituents and compounds of these wastes. Information on the chemical reaction products yielded in the cementitious materials was obtained using XRD and FT-IR. Differential scanning calorimetry (DSC) gave some kinetic parameters (onset and peak temperatures, and total reaction energy) of the exothermal acid-base reaction between -(-$NaPO_3$-)-$_n$ solution and CAC additive-blended BA. An image analysis using scanning electron microscopy (SEM) coupled with EDX captured the development of the microstructure and identified the chemical elements in the fractured solid cements.. Compressive strength tests were performed on cylindrical cement specimens with a diameter of 30 mm and a length of 60 mm; the results given are the average values of three specimens.

4. Results and Discussion

4.1 Chemical Analyses of Wastes

Table 1 gives the XPS surface chemical compositions of BA and WWTS powders after drying them for 24 hours at 120°C. The XPS measurement was made at an electron take-off angle of 40°, which corresponds to an electron-penetration depth of ~ 5.0 nm [9]; thus, the XPS data provide the atomic fractions present in the surface layer of ~ 5.0 nm thickness. The surface of the BA powders had 44.0 % O as the major atom, a moderate amount of S and C atoms, and lesser Ca, V, and Ni atoms. In contrast, the WWTS contained 42.6 % C and 35.8 % O as the principal atoms, and < 10% of S, Ca, V, and Ni as the minor ones. The C atom detected in the WWTS was associated mainly with the organic polyacrylamide additive that was incorporated as the heavy-metal absorbing reagent during the waste water treatment processes. XRD and FT-IR analyses also were conducted on these samples to identify their major chemical compounds. Figure 6 shows an XRD tracing for the BA, in a d-spacing range from 0.134 to 0.225 nm. It indicated the presence of two crystalline sulfate compounds, vanadium sulfate [$V_2(SO_4)_2$] [10] and calcium sulfate ($CaSO_4$) [11]. Correspondingly, its FT-IR spectral feature (Figure 7) over the frequency range of 4000-550 cm^{-1} strongly revealed that these bands represent the typical Ca- and V-related sulfate compounds [12]. Hence, the major chemical compounds of BA appear to be composed of $CaSO_4$ and $V_2(SO_4)_2$. Similar analytical results were obtained from the WWTS

(data not shown).

Since these wastes contain hazardous Ni and V metals, attention next was paid to their leachability from the wastes. Simply, the waste powder samples were immersed into the acid extraction solution and agitated for 18-24 hrs in accordance with TCLP. Then, the leachates were analyzed by AA to detect the concentrations of these metal ions. In this analytical work, we included other hazardous heavy metals such as As, Ba, Cd, Cr, Pb, Se, Hg, and Ag. Table 2 shows the total amounts of metals existing in the raw dry BA and WWTS wastes. The data were obtained in accordance with the following sequences: First, a 2 g waste sample was mixed into a 50 ml acid solution with pH < 2.0 at temperatures around 100°C, and then the mixture was agitated by magnetic stirrer for ~ 6 hours in attempting to digest completely the solid samples; second, the concentrations of these metallic ions digested in acid solution were estimated by AA; and finally, the gained ion concentrations for the respective metals were converted into the total mass, mg/kg. As is seen, the very large quantities of V and Ni ions appear to be present in these wastes; the amounts for V and Ni ranged from 47300-53000 mg/kg and 22500-30000 mg/kg, respectively. The Ba, Cr, and Pb, which were identified as being present in the second highest amounts ranged from 165 to 1030 mg/kg, while negligible amounts of < 100 mg/kg were detected from As, Cd, Hg, Se, and Ag. On the other hand, the concentrations of these metallic ions leached out from the raw BA and WWTS in accordance with TCLP are given in Table 3.

4.2 Pb-exchange Adsorbents (PES)

In trying to remediate Pb-contaminated soils, our emphasis centered on formulating and designing BA- and WWTS-based materials called Pb-exchange adsorbents (PEA) that not only can immobilize and stabilize Pb in the soils, but also fix Ni and V metals present in the raw wastes. Table 4 shows the formulations of PEA designed in this work. In these formulations, $Pb(NO_3)_2$ of chemical reagent grade was employed as the source of Pb, and 40 wt% was dissolved in a 60 wt% deionized water. Then, a certain amount of 40 wt% $Pb(NO_3)_2$ solution was added to each of the five different PEA slurry systems; BA-$NaPO_3$, BA-CSC-$NaPO_3$, BA-CAC-$NaPO_3$, WWTS-$NaPO_3$, and WWTS-CSC-$NaPO_3$. In preparing the specimens, the $Pb(NO_3)_2$-

incorporated PEA slurries were cast in the cylindrical molds (30 mm in diameter x 60 mm long) at room temperature and left for 1, 7, and 21 days in an atmospheric environment. The concentrations of Pb, Ni, and V ions leached out from the aged specimens were measured in accordance with the TCLP; the results for Pb are given in Table 5. The 1-day-aged Ba-$NaPO_3$ system (specimen No. 1) without any CSC and CAC additives liberated 0.88 mg/L. Since the amount of Pb present in this original PEA specimen containing 6.7 wt% [40 wt% $Pb(NO_3)_2$] was estimated as ~ 28800 mg/kg, this small amount liberated demonstrated that the BA-$NaPO_3$ system was highly effective in immobilizing Pb. When 1.3 wt% CSC additive was incorporated into the specimen No.1, the concentration of Pb leached out dropped ~ 36 % to 0.56 mg/L. Increasing the amount of CSC to 2.7 wt% led to a further decline to 0.49 mg/L. With a 5.3 wt% CSC, its leachability was determined to be < 0.4 mg/L. This information strongly suggested that the CSC additive serves to improve the performance of the BA-$NaPO_3$ system in immobilizing Pb. Contrarily, the efficacy of CAC additive in retaining Pb within the PEA bodies is lower than that of CSC. In fact, as is seen in the specimen No. 8, although a high concentration of 20.0 wt% CAC was added to the BA-$NaPO_3$, its leachability was 0.42 mg/L. Considerable attention was given to the WWTA-CSC-$NaPO_3$ system; namely, this system displayed a better performance on retaining Pb, rather than those of the BA-CSC-$NaPO_3$ and BA-CAC-$NaPO_3$ systems. The specimen No. 13 consisting of 53.8 wt% WWTS, 23.1 wt% CSC, and 23.1 wt% [40 wt% -(-$NaPO_3$-)-$_n$] was identified as the most promising PEA formulation in immobilizing Pb, allowing only 0.20 mg/L to leach out. The data also demonstrated that leaching of Pb tends to decrease with a lengthening time for all the PEA specimens

The V and Ni leachability test results for the four PEA systems, BA-$NaPO_3$, BA-CAC-$NaPO_3$, WWTS-$NaPO_3$, and WWTS-CSC-$NaPO_3$, are shown in Table 6. No attempt was made to detect these ions in BA-CSC-$NaPO_3$ system. In the BA-$NaPO_3$ system, the specimen No. 1 had a leachability of 425.0 mg/L and 16.0 mg/L for V and Ni ions, respectively. The quantities computed in the original specimens were 47300 mg/kg for V and 22500 mg/kg for Ni. Thus, this PEA system significantly inhibited the mobilization of these metals. As expected, the extent of their mobilization was further inhibited by adding CAC to the BA-$NaPO_3$ system; the 20 wt%

CAC-containing PEA system (specimen No. 8) had a leachability of 271.0 mg/L for V and 7.3 mg/L for Ni, corresponding to a 36.2 % and 54.7 % lowering, respectively, over those of the BA-$NaPO_3$ system without CAC. By comparison, a considerable reduction of both V and Ni leachability was obtained from the WWTS-CSC-$NaPO_3$ system; the specimen No. 13 containing 21.4 wt% CSC leached only 4.6 mg/L for V and 0.2 mg/L for Ni. The computed amounts of V and Ni present in this original specimen were 11130
mg/kg and 6300 mg/kg, respectively; thus, adding CSC to the WWTS-$NaPO_3$ system not only inhibits leaching of the Pb, but also greatly immobilizes the V and Ni in the raw WWTS. Unfortunately, a large amount of CSC cannot be incorporated into the BA-$NaPO_3$ system because CSC acts as a rapid-setting promoter of BA-based PEA. Therefore, the WWTS-CSC-$NaPO_3$ system was identified as the most effective PEA in immobilizing these metals, and was recommended for the remediation of Pb-contaminated soil.

4.3 High-performance Cements (HPC)

The ultimate goal in this work is to recycle the BA into cementitious materials that could be useful as a binder in building and civil engineering material systems. The ideal characteristics of such cements include a high compressive strength, rapid setting, and the intercalation of hazardous V and Ni metals present in the BA.

4.3.1 Exothermal Acid-Base Reaction

To gain data on the degree of reactivity of the $NaPO_3$ acid reactant with BA alone or with a BA/CAC mixture acting as the base reactant, and also on the exothermic energy generated by acid-base reaction between $NaPO_3$ and BA or BA/CAC, a DSC analysis was carried out using the non-isothermal method at a constant heating rate of 5 °C min^{-1} in a N_2 environment. Table 7 shows the mix formulations of the cements used in this study. The resulting DSC curve (see Figure 8) for all samples showed the typical exothermic features as a function of temperature. The enclosed area, A, of the curve with the baseline represents the total heat evolved during the exothermal reaction. Thus, the exothermic energy, ΔH (J/g), can be computed using the formula, $\Delta H = TRA/hm$, where T, R, A, h, and m refer to the temperature scale (°C in^{-1}), the range

sensitivity (mcal s^{-1} in^{-1}), the peak area (in^2), the heating rate (°C s^{-1}), and the sample's weight (mg), respectively. Also, we determined the two temperatures at which the DSC curves show the onset T_o, and peak T_p, of the exothermic reaction; the former, T_o, was estimated from the curves by finding the intersection point of two linear extrapolations. Table 8 compared such reaction parameters of these specimens. The onset T_o and peak T_p temperature, and the energy of exothermal reaction depend primarily on the amount of CAC additive incorporated into the BA; increasing the amount of CAC shifted in the T_o and T_p to a lower and higher temperature, respectively. Specimens with a BA/CAC ratio of 60/40 had the lowest T_o temperature of 48.46°C and the highest T_p temperature of 119.78°C in this test series. This information strongly verified that the extent of reactivity of $NaPO_3$ reactant to BA/CAC mixtures raised with an increasing amount of CAC; this means that the setting time of the cements was shortened as the proportion of BA to CAC was reduced. Concurrently, the comparison between the values of ΔH evolved by acid-base reaction demonstrated that ΔH increases with an increase in CAC content. The 60/40 ratio specimens had the highest ΔH of 130.60 J/g, corresponding to an ~ 3.4 time greater than that of the 100/0 ratio specimens without the CAC. Furthermore, these reaction parameters were correlated with the changes in compressive strength of the BA-based cement specimens developed in early curing stages at 2, 4, 7, and 24 hours after mixing at room temperature. In this experiment, the commercial Type I portland cement was used as the reference specimens which were prepared by mixing 70 wt% Type I cement and 30 wt% water. The results from these specimens are shown in Table 9. The data suggest that the development of strength for the BA cement specimens depends mainly on the BA-to-CAC ratio; decreasing this ratio led to an increasing strength. After a very limited curing period of 2 hours, there was no development of the strength in the 100/0 and 90/10 BA/CAC ratio specimens, nor in the control Type I cements. When 20 wt% of the total amount of BA was replaced by CAC, the 2-hr-aged-specimens displayed a compressive strength of 2.8 MPa. Further replacement by 30 wt% CAC increased the strength by ~ 3.8 % to 10.5 MPa. By comparison with this, no significant change in strength value was determined from the 60/40 ratio specimens, implying that the increase in strength seems to level off at about 70/30 ratio. Nevertheless, there is evidence that the incorporation of a proper amount of CAC additives into the BA-$NaPO_3$ cement system contributes to strengthening

the specimens at an early curing age, conferring rapid- hardening and -setting properties. Relating this information to the total energy, ΔH, (Table 8) evolved by exothermal acid-base reaction, it is likely that the ΔH value is one factor affecting the development of its strength; in fact, a high ΔH of > 100.0 J/g generated in the 70/30 and 60/40 ratio specimens was responsible for improving strength. The data also showed that the strengths of the specimens with a 80/20, 70/30, and 60/40 ratio tended to rise as curing time was prolonged. On the other hand, for the control specimens, a curing time of at least 7 hours was required to develop initial strength, and besides, the strength of 5.3 MPa at 7 hour age was ~ 2.2 times lower than that of the 70/30 ratio at the same curing time.

4.3.2 Compressive Strength

To gain more information on the optimized formulation of BA-based cements, two different experiments were carried out; one investigated the effect of -(-$NaPO_3$-)-$_n$ reactant in improving the compressive strength of the specimens, and the other related to the changes in strength of the specimens as a function of BA/CAC ratios. In these experiments, the specimens were cured by exposing them for 20 hours in steam at 80°C. The steam-curing technology was employed in response to attaining their ultimate compressive strength in a short curing time. In the first experiment, the same mix formulations of cement slurries as those used in assessing exothermal reaction energy were employed (see Table 7). The cement pastes were prepared by mixing these components at room temperature. After mixing, cement slurries were cast in cylindrical molds (30 mm in diameter x 60 mm long) and allowed to harden at 25°C in air for 24 hours. The hardened cement specimens were next exposed for 20 hours to 80°C steam. The results from the compressive strength test for these specimens are shown in Figure 9. The data indicated that the strength increases with an increasing concentration of -(-$NaPO_3$-)-$_n$ reactant in the cement systems. With the -(-$NaPO_3$-)-$_n$ of 40 wt%, the specimens had a compressive strength of ~ 35 MPa, corresponding to ~ 4 times higher than that of the specimens [0 wt% -(-$NaPO_3$-)-$_n$] made in the absent of -(-$NaPO_3$-)-$_n$. Since the maximum solubility of -(-$NaPO_3$-)-$_n$ at 25°C is ~ 81 g in a 100 g water, the 40 wt% -(-$NaPO_3$-)-$_n$ solution is nearing its saturation point. Hence, this concentration of -(-$NaPO_3$-)-$_n$ reactant was selected for further research on optimizing the

cement formulation. The plots of compressive strength versus BA/CAC ratio for the steam-cured specimens with a constant concentration of 40 wt% -(-$NaPO_3$-)-$_n$ are given in Figure 10. The data showed that the strength markedly increases between the BA/CAC ratios of 100/0 and 70/30, and then gradually rises between the 70/30 and 60/40 ratios. The specimens made with the 70/30 ratio had a compressive strength of 34.8 MPa, reflecting an improvement of more than 23 times over those without CAC (100/0 ratio). There was no significant difference in strength between the 70/30 and 60/40 ratio specimens. In fact, the compressive strength of the latter, 36.5 MPa, was only ~ 5.0 % higher than that of the 70/30 ratio. From all this information, a cement system consisting of a 42 wt% BA, 18 wt% CAC, 24 wt% water, and 16 wt% -(-$NaPO_3$-)-$_n$, was identified as the most effective formulation in providing quick-setting properties and in developing high compressive strength.

Using this formulation, attention next centered on examining the changes in strength of the cement specimens as a function of curing times for up to 28 days in air or water at room temperature. By comparison, the commercial Type I portland cement specimens were used as controls. Figure 11 plots compressive strength versus curing time for the BA and Type I cement specimens cured in air or water. The data reveal that the behavior of strength development for the BA cement specimens, except during early curing times up to 24 hours, was very similar to that for the commercial Type I portland cement specimens; namely, the compressive strength of the specimens cured in water was much higher than that in air, and the strength increased with an increasing curing time. Also, there was no significant difference between the maximum strengths of the 28-day-aged BA and Type I cement specimens.

4.3.3 Phase Identification and Development of Microstructure

To obtain insights into the phase composition and transformation, and the development of microstructure that are responsible for strengthening the BA cement, XRD and SEM-EDX analyses were carried out for the BA-$NaPO_3$ and BA-CAC-$NaPO_3$ systems after curing for 28 days in air and water at 25°C, and for 20 hours in 80°C steam. Figure 12 shows the XRD d-spacing patterns, ranging from 0.134 to 0.225 nm, for these powder samples, and also includes

the spacing patterns of the CAC additive (a) and the raw BA powder (b) as the reference samples. The XRD tracing for the CAC reference sample revealed the presence of three major components; monocalcium aluminate ($CaO.Al_2O_3$) [13], gehlenite ($2CaO.Al_2O_3.SiO_2$) [14], and monocalcium dialuminate ($CaO.2Al_2O_3$) [15]. In the BA-$NaPO_3$ system, the diffraction pattern (c) of the specimens cured in air for 28 days exhibited features similar to those of the reference BA, except for the elimination and a considerable decrease in line intensity of the $CaSO_4$-related d-spacings at 0.345, 0.324, 0.302, and 0.283 nm. When this cement system was cured in steam, the interesting diffraction features (d), compared with those of the raw BA and 28-day-air-cured specimens, were as follows: (1) the appearance of new d-spacings at 0.380, 0.336, 0.330, 0.328, 0.281, 0.277, 0.272, and 0.268 nm, and (2) the declining line intensity of the peaks originating from $V_2(SO_4)_3$. Referring to the result (1), all four new lines at 0.380, 0.336, 0.330, and 0.328 nm were assigned to the formation of sodium vanadium sulfate hydrate [SVSH, $Na_2V(SO_4)_2.4H_2O$] [16], and the remaining four lines revealed the formation of hydroxyapatite [HOAp, $Ca_5(PO_4)_3(OH)$] [17]. Therefore, we assumed that the HOAp phase perhaps was precipitated by an interaction between the Ca ions liberated from hydrolysis of $CaSO_4$ and the phosphate anion from the $-(-NaPO_3-)-_n$; meanwhile Na as a counter ion of the phosphate anion reacted with the $V_2(SO_4)_3$ to form SVSH in the hydrothermal environments. These reaction products yielded by the hydrothermal reactions between the $-(-NaPO_3-)-_n$ and the $CaSO_4$ or $V_2(SO_4)_3$ are likely to be responsible for strengthening the BA-$NaPO_3$ specimens.

In the BA-CAC-$NaPO_3$ system, the pattern (e) of 28-day-air-cured specimens showed that two crystalline reaction products are formed in the cement bodies: SVSH and HOAp, while non-reactive BA- and CAC-related compounds, such as $V_2(SO_4)_3$, $CaSO_4$, $CaO.Al_2O_3$, and $2CaO.Al_2O_3.SiO_2$ still remain. Since these reaction products do not form in the BA-$NaPO_3$ system under the same curing conditions [see pattern (c)], it is possible to rationalize that the formation of HOAp is more likely to be associated with the Ca ion dissociated from the CAC additive, rather than that from $CaSO_4$. In other words, the interaction between the Ca ions liberated from CAC and the phosphate ions from the $-(-NaPO_3-)-_n$ led to the introduction of HOAp phase. Concurrently, the Na counter ions favorably reacted with $V_2(SO_4)_3$ to yield the

SVSH phase. If this interpretation is valid, the CAC additive acts to promote the formation of these crystalline reaction products. By comparison, the pattern's feature of the 28-day-water-cured specimens (f) was characterized by representing a striking reduction of these unreactive compound-associated line intensities, except for $2CaO.Al_2O_3.SiO_2$, and an increase in the line intensity of the HOAp and SVSH phases. This information highlights two important factors affecting the improvement of its mechanical strength: One was that the CaO component in the $CaO.Al_2O_3$ and $CaO.2Al_2O_3$ phases present in the CAC additive has a higher rate of reactivity with the $-(-NaPO_3-)-_n$ than that in the $2CaO.Al_2O_3.SiO_2$ phase; the other factor reflected the information of a well-crystallized SVSH and HOAp phases, implying that a long-term immersion of the specimens into the water led to increasing their degree of hydration. Thus, there is no doubt that the cements were formed through the two-step reaction pathways, acid-base and hydration, and act to bind the partially reacted and nonreactive BA and CAC particles into a coherent mass. A similar pattern was depicted from the specimens (g) cured in steam. Relating these data to the compressive strength described earlier, the assemblage of two well-formed reaction products, HOAp and SVSH, in the cement bodies, significantly contributed to conferring a high compressive strength to the BA-based cement specimens.

This information was substantially supported by exploring the development of microstructure and inspecting the elemental distribution of the fractured surfaces of the cement specimens used in the XRD analyses. Figure 13-a shows SEM micrograph for the 28-day-air-cured BA-$NaPO_3$ specimens. Its morphological features were characterized by disclosing the coverage of the BA reactant surfaces by the particles ranging from 0.1 to 0.4 μm. These particles are explicable as the reaction products of $-(-NaPO_3-)-_n$ with BA. In fact, the EDX spectrum (not shown) of the particles had a principal Ca signal, together with the predominant peak of P, representing the formation of the calcium phosphate compounds as the reaction products. Correlating this finding with an earlier XRD result (Figure 12-c), such reaction products serving as the binder in this cement system, appear to be substantially amorphous phases. The SEM image also revealed the porous microstructure, reflecting its weak mechanical strength. A striking alteration in the microstructure occurred when this cement system was cured in steam

(Figure 13-b): there is a coalescent microstructure of these particles. Such treatment led to the conversion of porous microtexture into a dense one, so improving the mechanical strength of the cement specimens.

In the BA-CAC-$NaPO_3$ system, the SEM image of the 28-day-air-cured specimens (Figure 13-c) had two discernable morphologies: The first was the coverage of the BA and CAC reactant surfaces by particle reaction products; the second was the agglomerated microstructure of these particles. In contrast, a quite different structure was observed from the specimens (Figure 13-d) cured for 28 days in water; the SEM revealed a striking image of a highly densified bulky microstructure because of the smooth surface texture disclosed on the fractured surfaces. This densified microstructure appears to be developed by the hydration of reaction products when the specimens are immersed in water; it accounted for the increase in mechanical strength of the specimens, compared with that of the specimens cured in air. As expected, the morphological texture (not shown) taken from the fractured surfaces of the steam-cured specimens closely resembled that of the 28-day-water-cured specimens. In addition, a well-formed calcium phosphate crystal compound was observed in the cavities of fractured specimens. Figure 14 shows a SEM image specifically expressing a randomly distributed sphere-shaped crystalline compound, and an agglomeration of individual spherical crystals, ranging from 0.4 to 1.5 μm. The SEM close examination of these spheres revealed that they are composed of an entangled, interlocked structure of well-grown flake-like crystals. EDX is extremely useful for quantitative analysis of individual elements on a solid surface layer, up to ~ 1.5 μm thick. The abscissa of the EDX spectrum is the X-ray energy characteristic of the element, and the intensity of the gross peak count relates directly to the amount of each element present. Therefore, EDX techniques for subsurface analyses can greatly facilitate the interpretation of SEM images. The EDX spectrum concomitant with SEM for the spherical crystal, denoted as site "A", indicated an elemental distribution consisting of calcium and phosphate as the major components, and aluminum, silicon, and vanadium as minor ones. No S element was detected in this area. Thus, the spherical crystals are more likely to be accounted for by calcium phosphate hydrates, perhaps, the HOAp phase, rather than the SVSH phase. The image also expressed the growth of small flake-like

crystals in the open spaces between the spherical crystals. The EDX spectrum of these crystals, denoted as site "B", included four dominant elements, aluminum, silicon, phosphate, and calcium. Since the depth of X-ray penetration for the EDX is ~ 1.5 μm, although the flake-like crystals are associated with the calcium phosphate compounds, the two remaining elements, Al and Si, may arise from the underlying CAC additives.

5. Conclusion

In attempting to seek the potential applications for waste water treatment sludge (WWTS) and boiler ash (BA) generated from KeySpan's power stations, and also to deal with these industrial by-products, we succeeded in recycling them into two viable products; Pb-exchange adsorbents (PEAs) and high-performance cements. These products were made from chemically bonded cement and ceramic (CBC) materials, which were synthesized through the two-step chemical reaction pathways, acid-base and hydration. Using this synthesis technology, both the WWTS and BA served in acting as the solid base reactants, and the sodium polyphosphate, [-(-$NaPO_3$-)-$_n$] , known as an intermediator of fertilizer, was employed as the acid solution reactant. In addition, two commercial cement additives, Refcon as calcium aluminate cement (CAC) and Type I as calcium silicate cement (CSC), were also used to improve mechanical behavior and to promote the rate of acid-base reaction of the CBC materials.

With regards to PEA, not only do the synthesized CBCs remediate Pb-contaminated soils, they acted to immobilize and stabilize hazardous heavy metals, such as vanadium (V) and nickel (Ni), which are contained in these raw by-products. In fact, using a CBC formulation consisting of 53.8 wt% WWTS, 23.1 wt% CSC, and 23.1 wt% [40 wt% -(-$NaPO_3$-)-$_n$], TCLP tests showed that the concentrations of Pb, Ni, and V metals leached out from the specimens containing ~ 28800 mg/kg of Pb, ~ 6300 mg/kg of Ni, and ~ 11130 mg/kg of V, into the acid extraction fluid, were only 0.15 mg/L of Pb, 0.15 mg/L of Ni, and 4.63 mg/L of V. On the other hand, the BA-CAC-$NaPO_3$ system-based CBCs had a high potential for use as HPCs, offering a high mechanical strength, quick-setting characteristics, and a binding matrix of V and Ni metals present in the BA. Since the CAC additive acts to promote the rate of acid-base reaction,

incorporating the base reactant with 70/30 BA/CAC ratio into the -(-$NaPO_3$-)-$_n$ acid reactant generated a high exothermal reaction energy, leading to rapid hardening and setting, as the cement slurry was converted into a solid state within the first ten minutes after mixing. This 70/30 ratio specimens cured for 2 hours after mixing had a compressive strength of 10.5 MPa. Further, the excellent compressive strength of > 33.0 MPa for this cement system was attained when the cement specimens were cured by immersing them for 20 hours in 80°C steam. Two important factors played a key role in providing such a high compressive strength: One was the formation of both well-crystallized hydroxyapatite [HOAp, $Ca_5(PO_4)_3(OH)$] and sodium vanadium sulfate hydrate [SVSH, $(Na_2V(SO_4)_2.4H_2O)$] in the cement bodies; the other was associated with the development of densified cement microstructure. These reaction products may be formed by the following hypothetical reaction mechanisms:

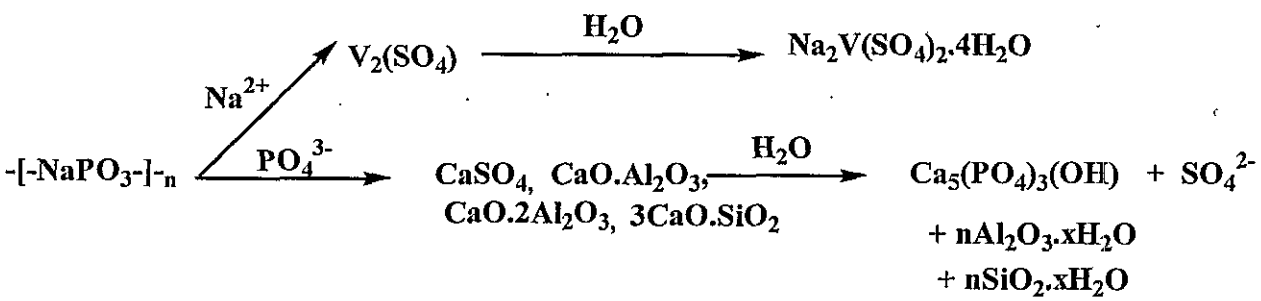

First, the Ca cations liberated from the BA and CAC had a strong chemical affinity for the phosphate anions dissociated from the -(-$NaPO_3$-)-$_n$ acid solution, leading to the formation of calcium phosphate compounds. Second, Na cations as the counter anions of phosphate ions favorably reacted with $V_2(SO_4)_3$ present in the BA to yield the sodium vanadium sulfate compounds. Finally, the hydration of these reaction products contributed to promoting their crystallization, thereby developing a dense microstructure in the CBC. In this mechanism, three compounds, SO_4^{2-}, $nAl_2O_3.xH_2O$, and $nSiO_2.xH_2O$, may be formed as by-products in this acid-base-hydration reaction process. Overall, we believe that the CBCs derived from these wastes

have a great potential for use as the remediating materials for soil contaminated with hazardous Pb metal, as rapid-setting repair patching and filling materials for damaged roadways and bridges, and as well as high strength precast concrete products, such as building blocks, pipes, and slabs. The results show them to be not only an environmentally safe and economic solution to the problem of disposing these wastes, but the materials also may accrue revenue from their sale as end-use products.

References

1. T. Sugama and N.R. Carciello, Cem. Concr. Res., 23, 1409 (1993).
2. T. Sugama, Cem. Concr. Res., 26, 1661 (1996).
3. T. Sugama, Adv. Cem. Res., 9, 65 (1997).
4. T. Sugama, M. Allan, and J.M. Hill, J. Am. Ceram. Soc., 75, 2076 (1992).
5. A.M. Rouhi, Chemical & Engineering News, 76, January 13, 21 (1997).
6. A.W. Adanson, "A Textbook of Physical Chemistry", p.1015, Academic Press, New York (1983).
7. J.C. Bolger, in : Adhesion Aspects of Polymeric Coatings, K.L. Mittal (Ed.) p. 3, Plenum Press, New York (1983).
8. G.A. Parke, Chem. Rev. 65, 177 (1965).
9. M.P. Seah and W.A. Dench, Surf. Interface Anal., 1, 2 (1979).
10. Powder Diffraction File, Inorganic Phases, JCPDS 27-942, (1984).
11. Powder Diffraction File, Inorganic Phases, JCPDS 30-279, (1984).
12. R.A. Nyquist and R.O. Kagel, "Infrared Spectra of Inorganic Compounds", pp. 268-275, Academic Press, New York, (1971).
13. Powder Diffraction File, Inorganic Phases, JCPDS 23-1036 (1984).
14. Powder Diffraction File, Inorganic Phases, JCPDS 20-199 (1984).
15. Powder Diffraction File, Inorganic Phases, JCPDS 23-1037 (1984).
16. Powder Diffraction File, Inorganic Phases, JCPDS 25-885 (1984).
17. Powder Diffraction File, Inorganic Phases, JCPDS 9-432 (1984).

Table 1. XPS Surface Chemical Analysis at BNL for BA and WWTS generated from KeySpan's Power Stations

	Atomic fraction, %					
	S	C	Ca	O	V	Ni
BA	12.4	29.3	8.0	44.0	4.1	2.2
WWTS	8.0	42.6	4.6	35.8	6.2	2.8

Table 2. Amounts of total metals existing in the dry BA and WWTS wastes

	Amount, mg/kg									
	As	Ba	Cd	Cr	Pb	Hg	Se	Ag	V	Ni
BA	30	745	7	155	464	<0.25	4	2	47300	22500
WWTS	84	1030	15	269	760	<1	20	<6	53000	30000

Tabe 3. Concentrations of metals leached out from the BA and WWTS in accordance with TCLP

	As	Ba	Cd	Cr	Pb	Hg	Se	Ag	V	Ni
BA	49.7 μg/L	0.2 mg/L	0.11 mg/L	0.1 mg/L	0.22 mg/L	<0.5 μg/L	9.4 μg/L	0.02 mg/L	508 mg/L	16 mg/L
WWTS	8.6 μg/L	0.4 mg/L	0.03 mg/L	0.03 mg/L	< 0.06 mg/L	<0.5 μg/L	44.6 μg/L	<0.02 mg/L	11.9 mg/L	41.8 mg/L

Table 4. Mix formulations of the KeySpan waste-based cements

Specimen No.	Formulation* wt%					
	BA	WWTS	CSC	CAC	40wt%-(-$NaPO_3$-)-$_n$	40wt%Pb(NO_3)$_2$
1	66.7	-	-	-	26.6	6.7
2	65.4	-	1.3	-	26.6	6.7
3	64.0	-	2.7	-	26.6	6.7
4	62.7	-	4.0	-	26.6	6.7
5	61.3	-	5.3	-	26.6	6.7
6	60.0	-	-	6.7	26.6	6.7
7	53.3	-	-	13.3	26.6	6.7
8	46.7	-	-	20.0	26.6	6.7
9	-	71.4	-	-	21.4	7.2
10	-	67.9	3.5	-	21.4	7.2
11	-	64.3	7.1	-	21.4	7.2
12	-	57.1	14.3	-	21.4	7.2
13	-	50.0	21.4	-	21.4	7.2

*BA :boiler ash

WWTS :waste water treatment sludge

CAC :calcium aluminate cement additive

CSC :calcium silicate cement additive

40wt%-(-$NaPO_3$-)-$_n$: 40 wt% granular polybasic sodium phosphate and 60 wt% water

Table 5. Pb leachability from $Pb(NO_3)_2$-incorporated cements after curing for 1, 7, and 21 days at room temperature

Specimen No.	Pb leachability, mg/L		
	1 day	7 days	21 days
1	0.88	0.69	0.54
2	0.56	0.42	0.33
3	0.49	0.36	0.29
4	0.40	0.30	0.24
5	0.38	0.28	0.21
6	0.79	0.56	0.41
7	0.75	0.51	0.32
8	0.42	0.31	0.29
9	0.39	0.30	0.25
10	0.38	0.29	0.23
11	0.36	0.27	0.20
12	0.25	0.20	0.18
13	0.20	0.15	0.15

Table 6. Pb, V, and Ni leachability of 21-day-aged cements

Specimen No.	Leachability, mg/L		
	Pb	V	Ni
1	0.54	425.0	16.0
7	0.32	324.0	9.5
8	0.29* (0.99)	271.0	7.25
9	0.25	506.0	145.0
11	0.20	84.0	28.4
13	0.15	4.6	0.15

* BNL value

Table 7. Mix formulations of cement slurries

Concentration of -(-NaPO3-)-n, wt%	Mix formulation* wt%			
	BA	CAC	Water	-(-NaPO3-)-n
0	42	18	40	-
10	42	18	36	4
20	42	18	32	8
30	42	18	28	12
40	42	18	24	16

* BA :boiler ash

CAC :calcium aluminate cement additive

$-(-NaPO_3-)-_n$:granular polybasic sodium phosphate

Table 8. Exothermal reaction parameters of the 100/0, 90/10, 80/20, 70/30, and 60/40 BA/CAC ratio specimens

BA/CAC ratio	Exothermal reaction		
	Onset temperature, T_o, °C	Peak temperature, T_p, °C	Total energy, ΔH, J/g
100/0	70.06	113.06	38.78
90/10	60.32	114.82	73.45
80/20	57.15	115.53	88.15
70/30	50.35	116.25	110.36
60/40	48.46	119.78	130.60

Table 9. Compressive strength of the specimens with different BA/CAC ratios and the Type I portland cement specimens at early curing times for up to 24 hours

Cement	Compressive strength, MPa			
	2 hrs	4 hrs	7 hrs	24 hrs
Type I	*	*	5.3	6.8
BA/CAC 100/0	*	*	*	2.6
BA/CAC 90/10	*	*	5.6	7.0
BA/CAC 80/20	2.8	4.6	6.7	8.2
BA/CAC 70/30	10.5	11.0	11.4	12.3
BA/CAC 60/40	10.8	11.4	11.8	12.9

* Too weak to be measured.

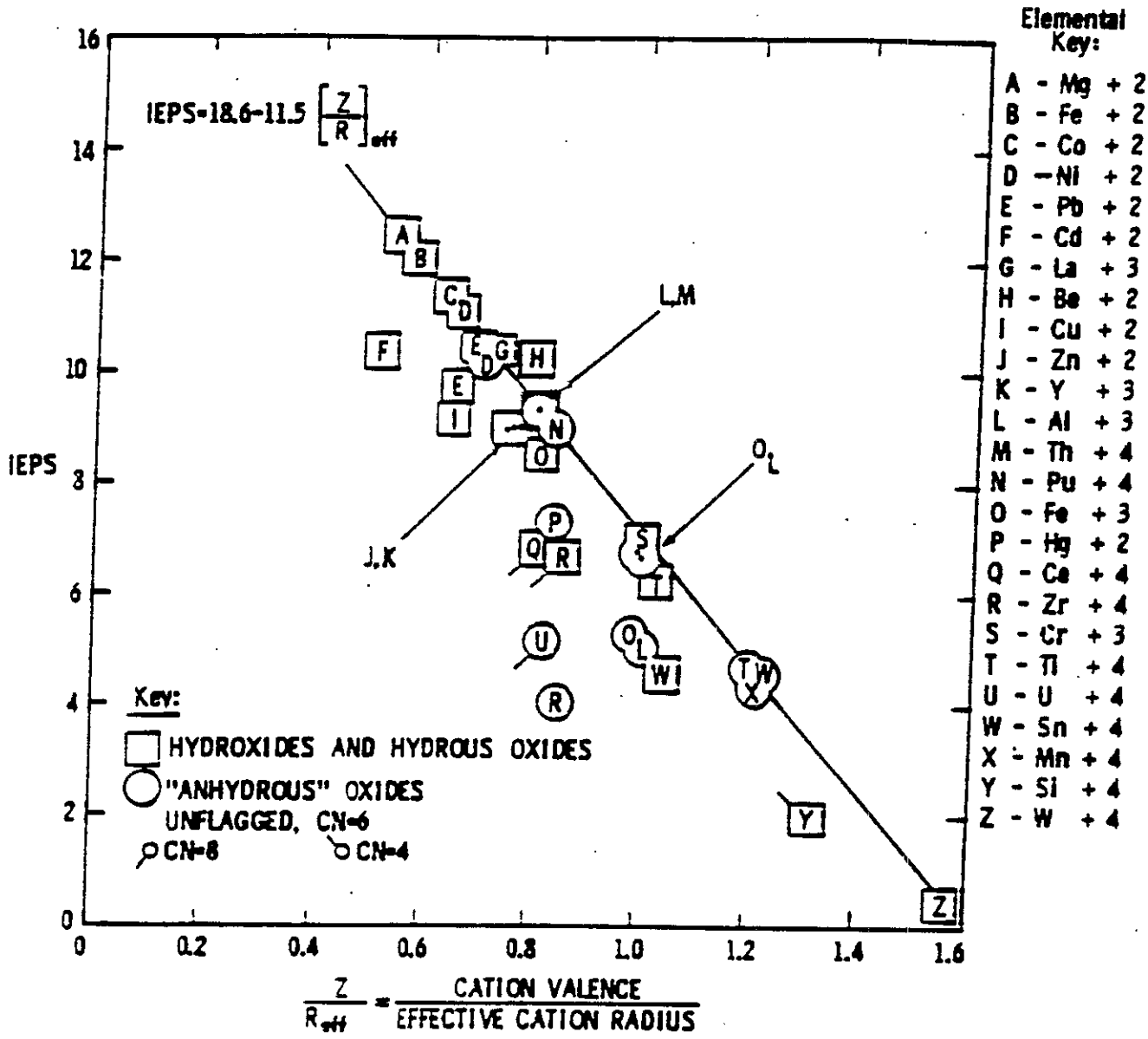

Figure 1. Parks's equation for the isoelectric point (IEPS) of particle surfaces

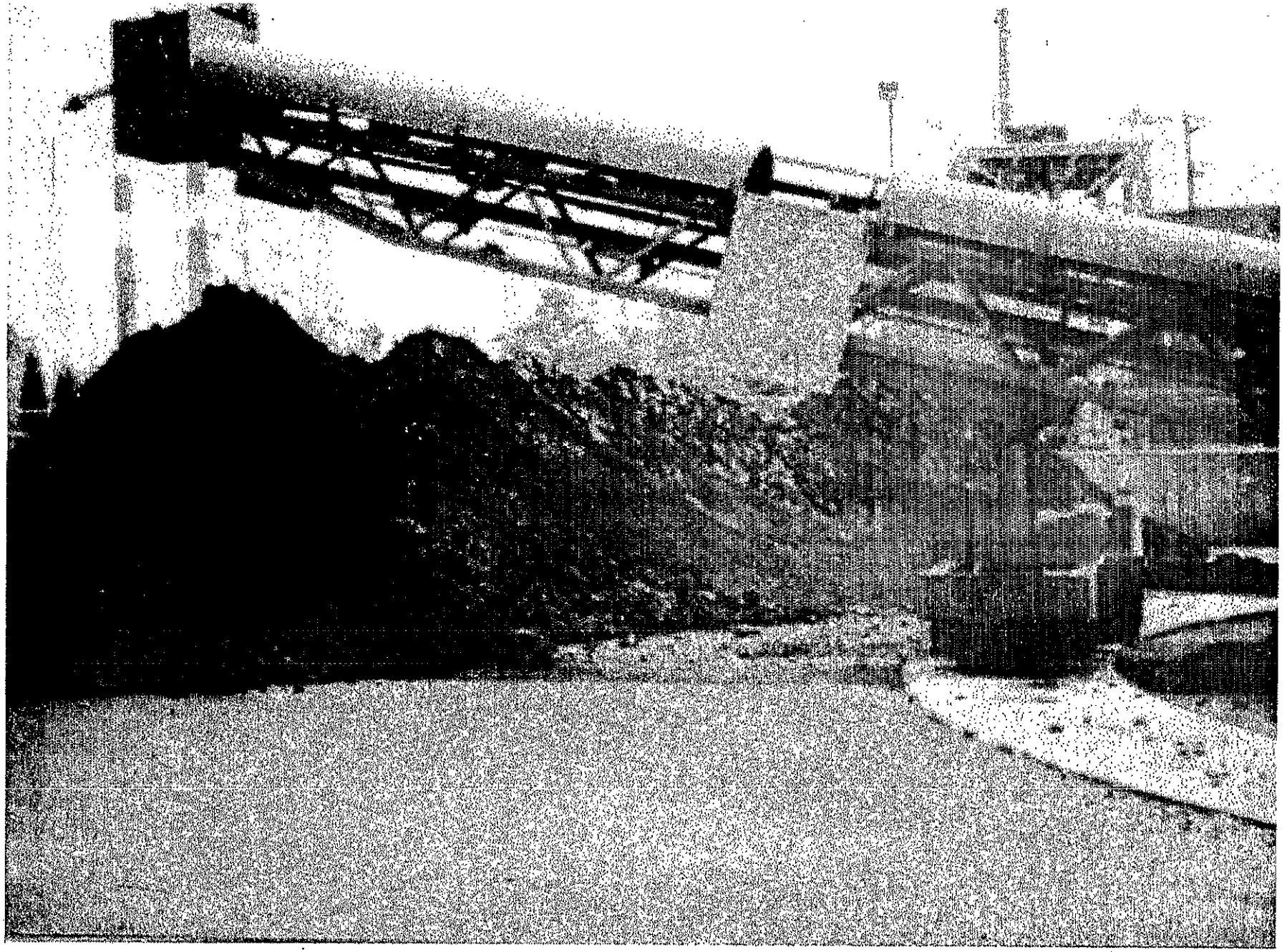

Figure 2. Waste water treatment sludge (WWTS) from KeySpan's power plants

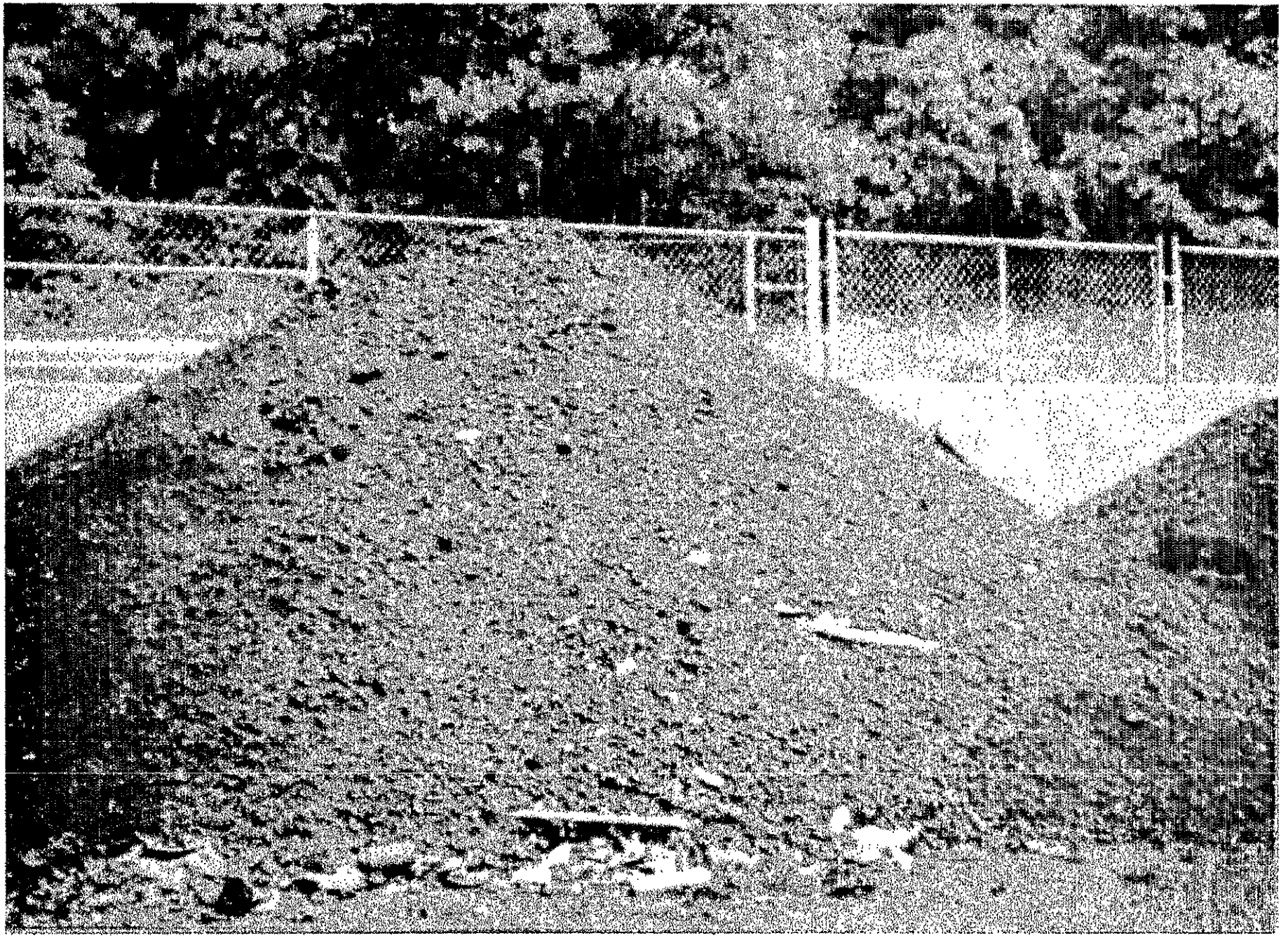

Figure 3. Boiler ash (BA) generated from KeySpan's power plants

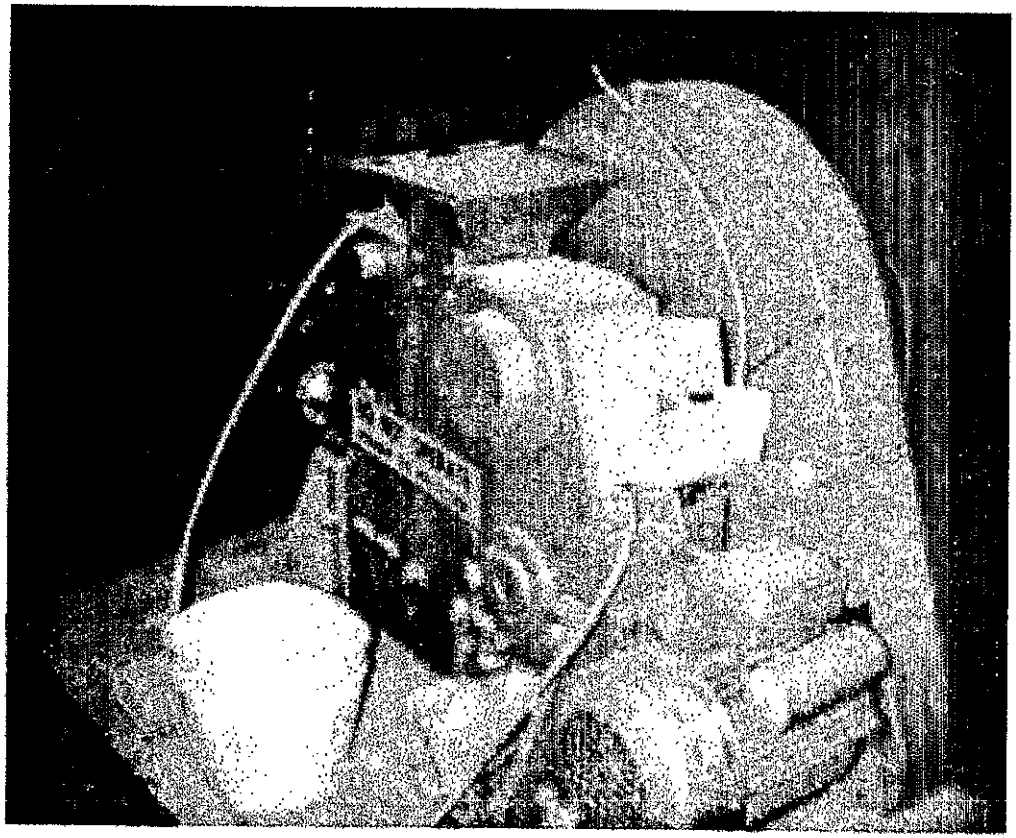

Figure 4. Crusher used to convert bulky BA into powders

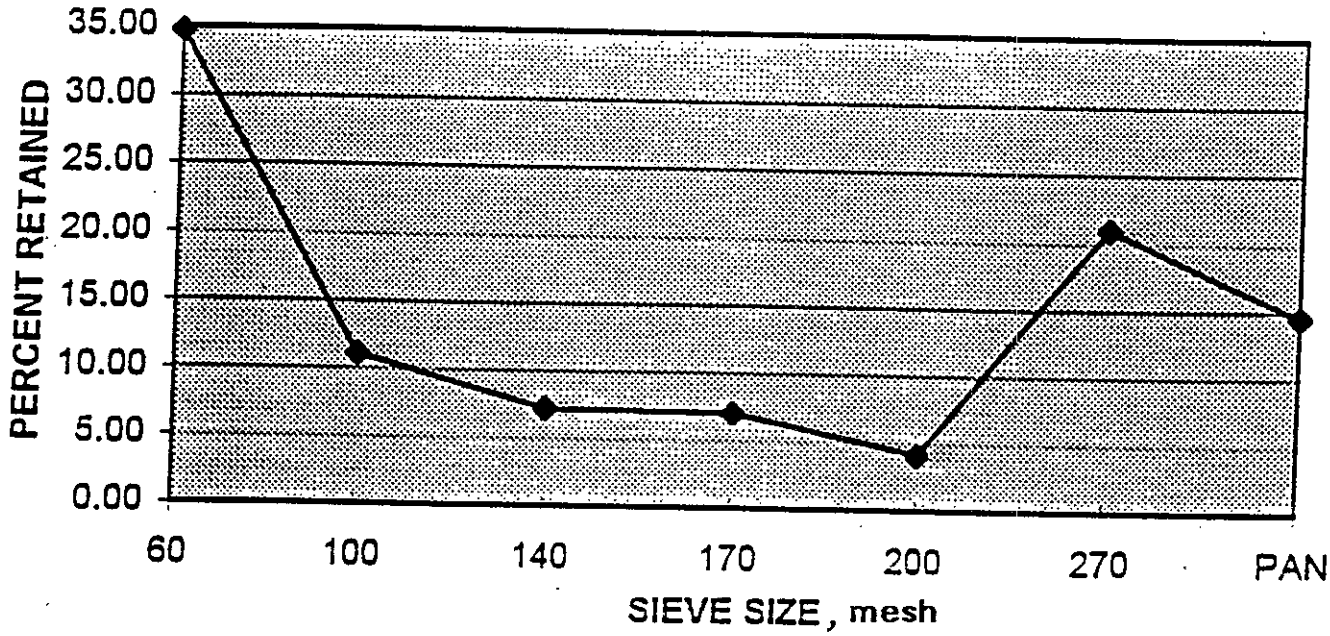

Figure 5. Sieve size analysis of crushed BA powders

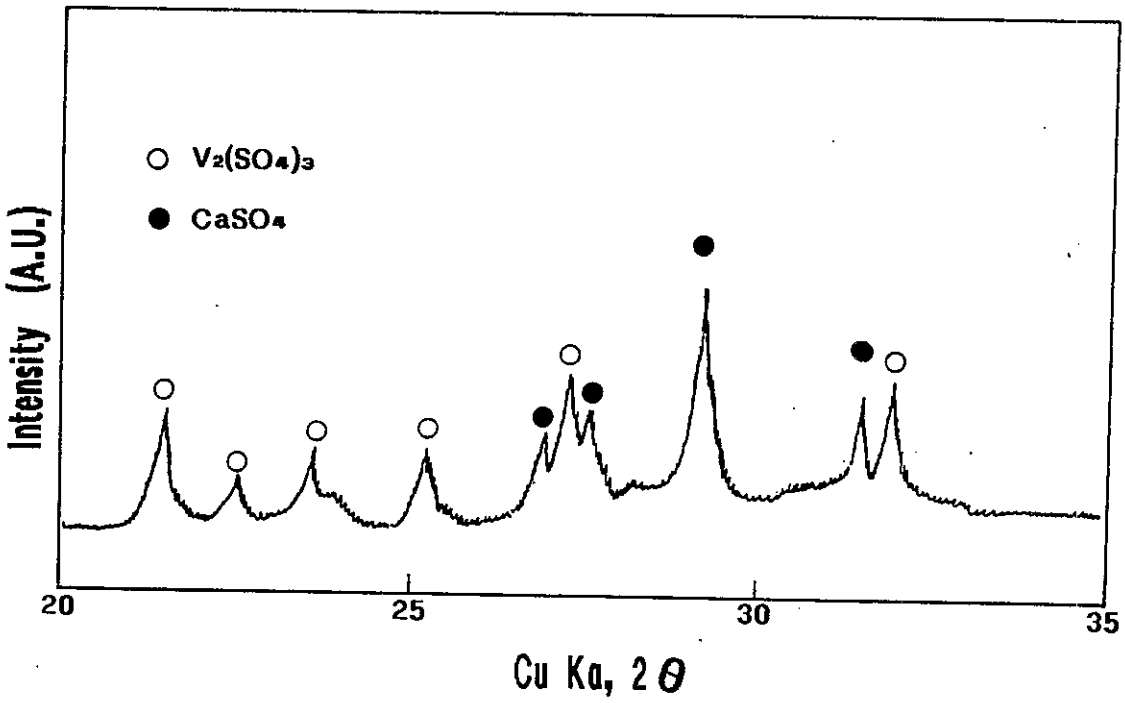

Figure 6. XRD pattern of crushed BA powders

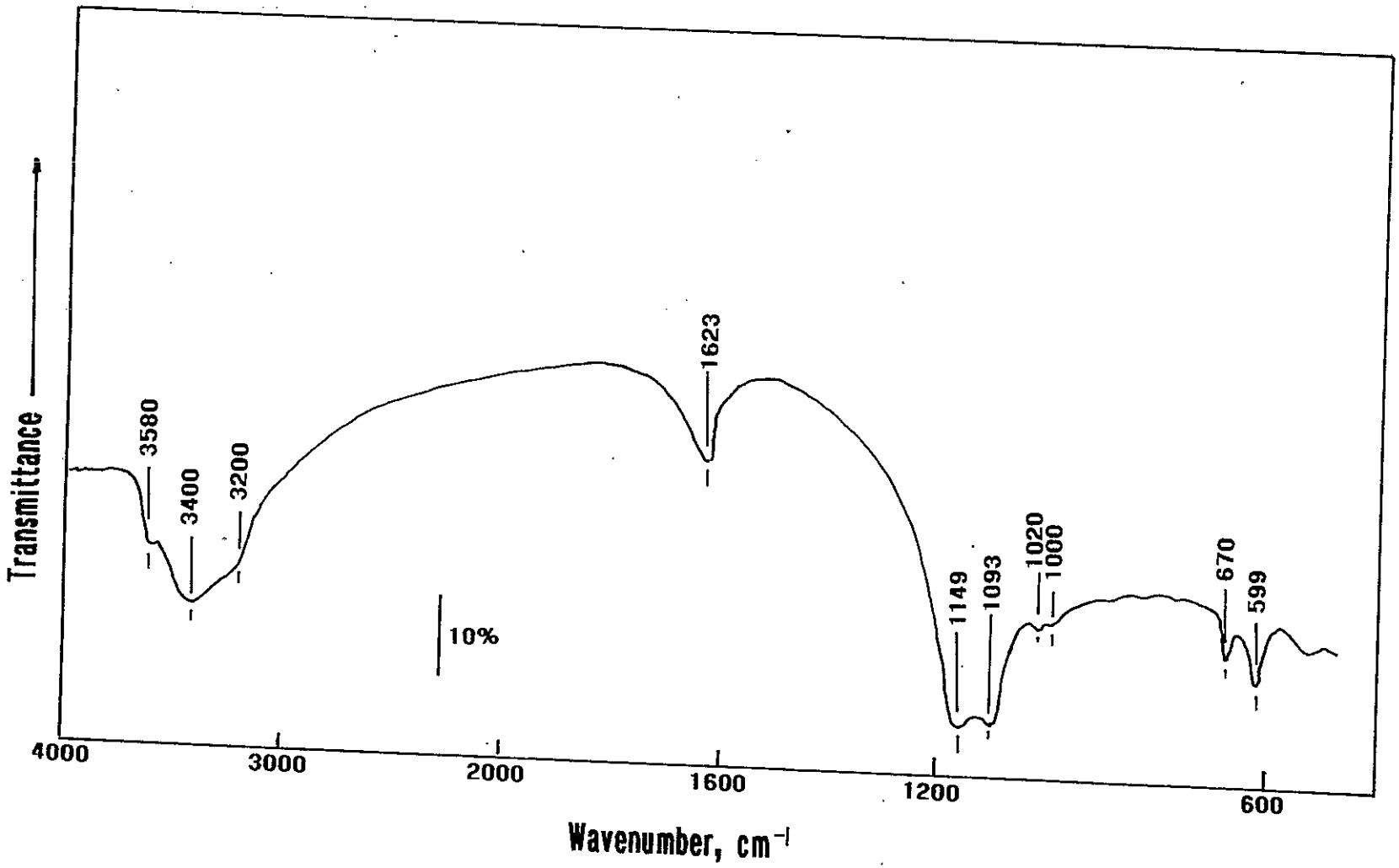

Figure 7. FT-IR spectrum of BA powders

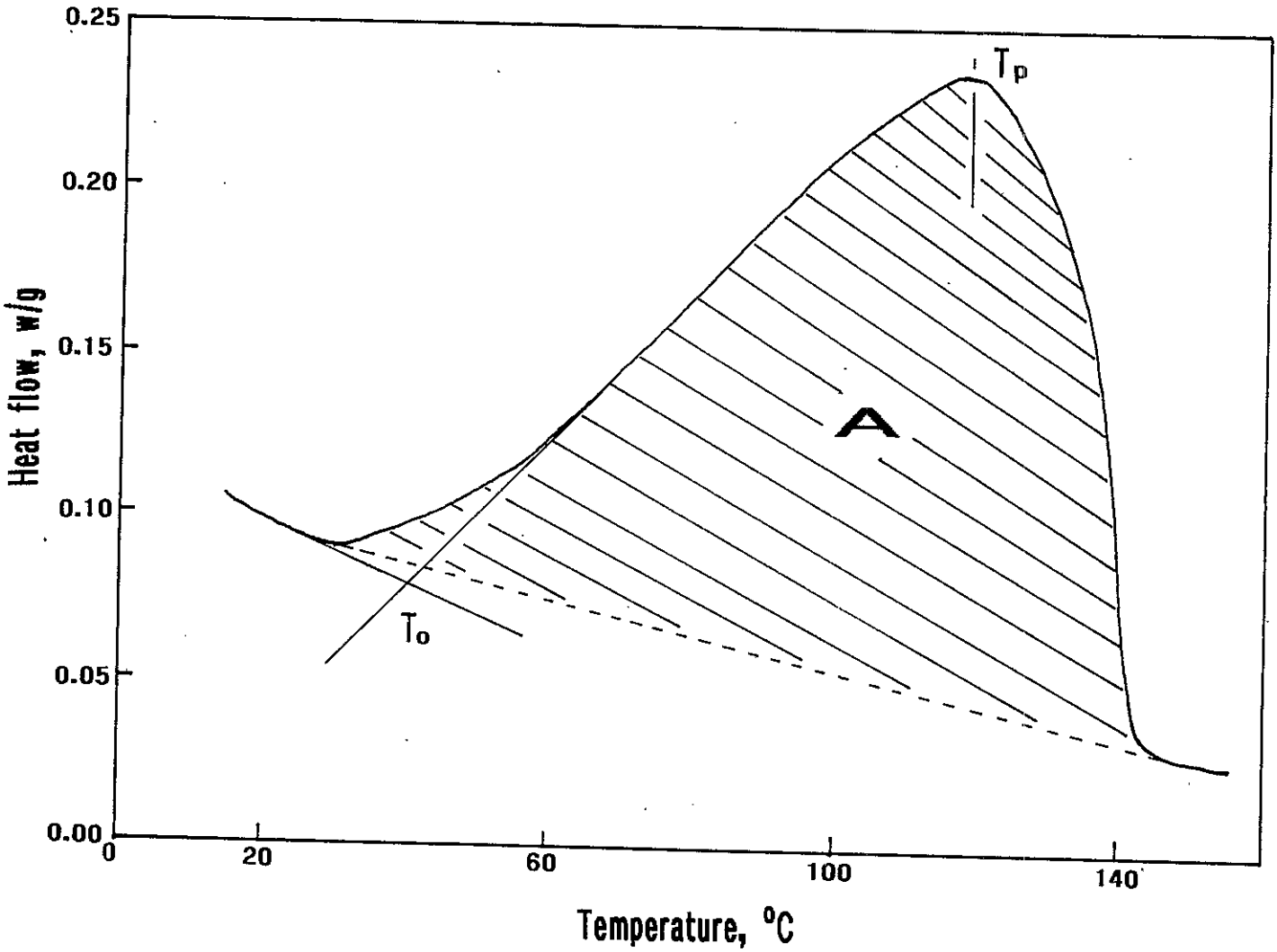

Figure 8. Non-isothermal DSC curve showing total acid-base exothermal reaction energy

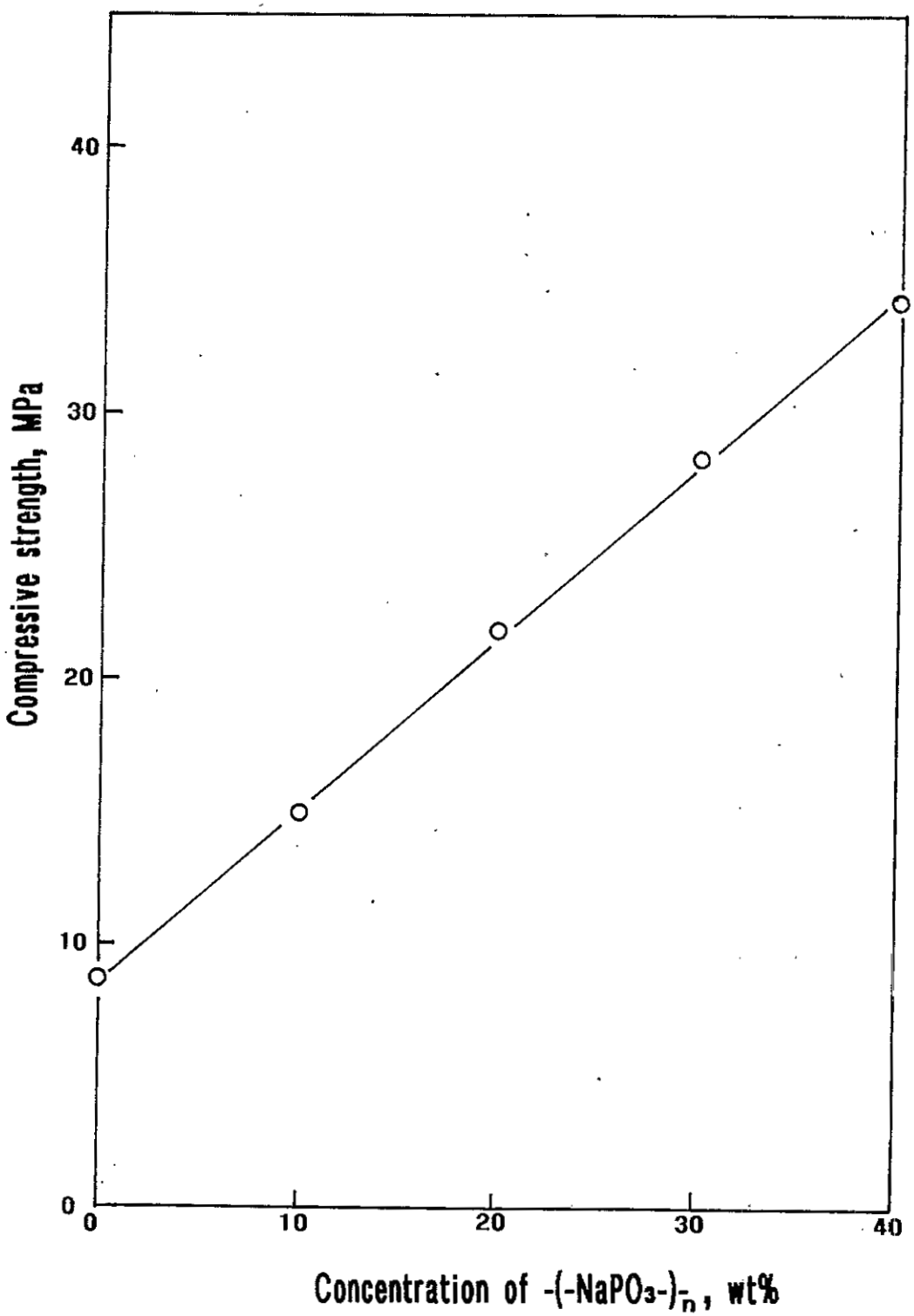

Figure 9. Compressive strength versus concentration of -(-$NaPO_3$-)-$_n$

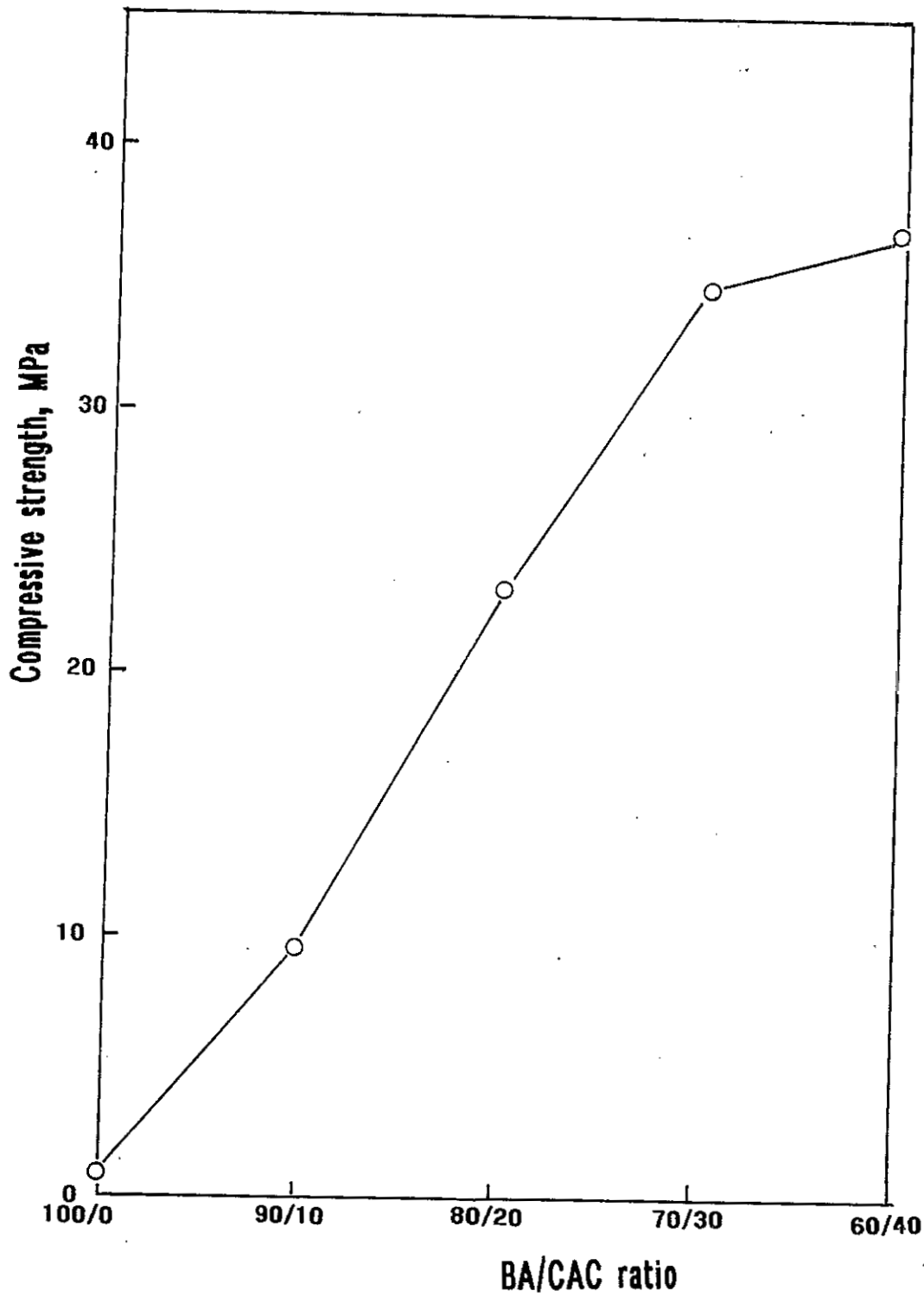

Figure 10. Changes in compressive strength for the 80°C-autoclaved cement specimens as function of BA/CAC ratio

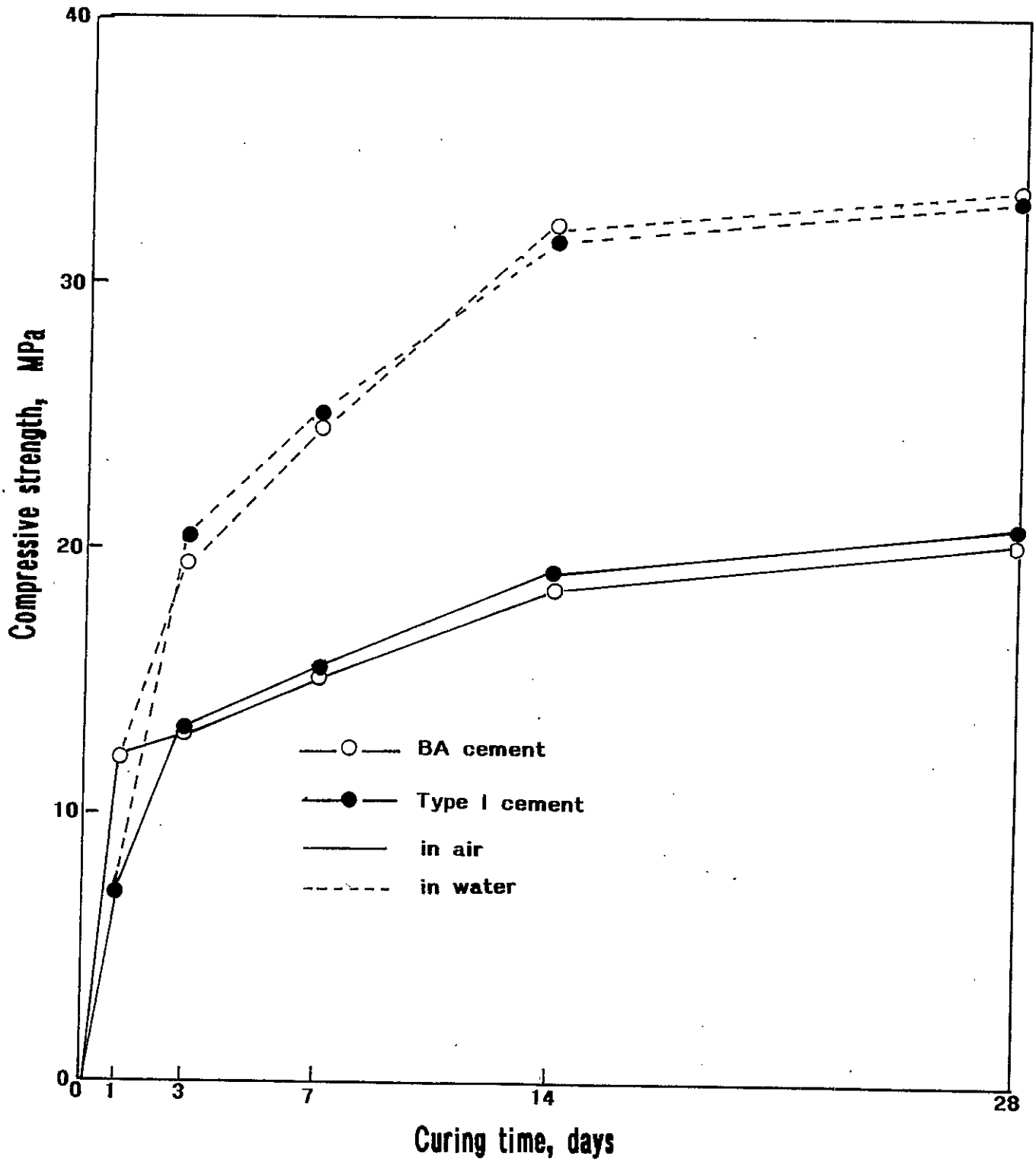

Figure 11.Changes in compressive strength for BA cement and commercial Type I cement specimens as function of curing time in air or water at room temperature

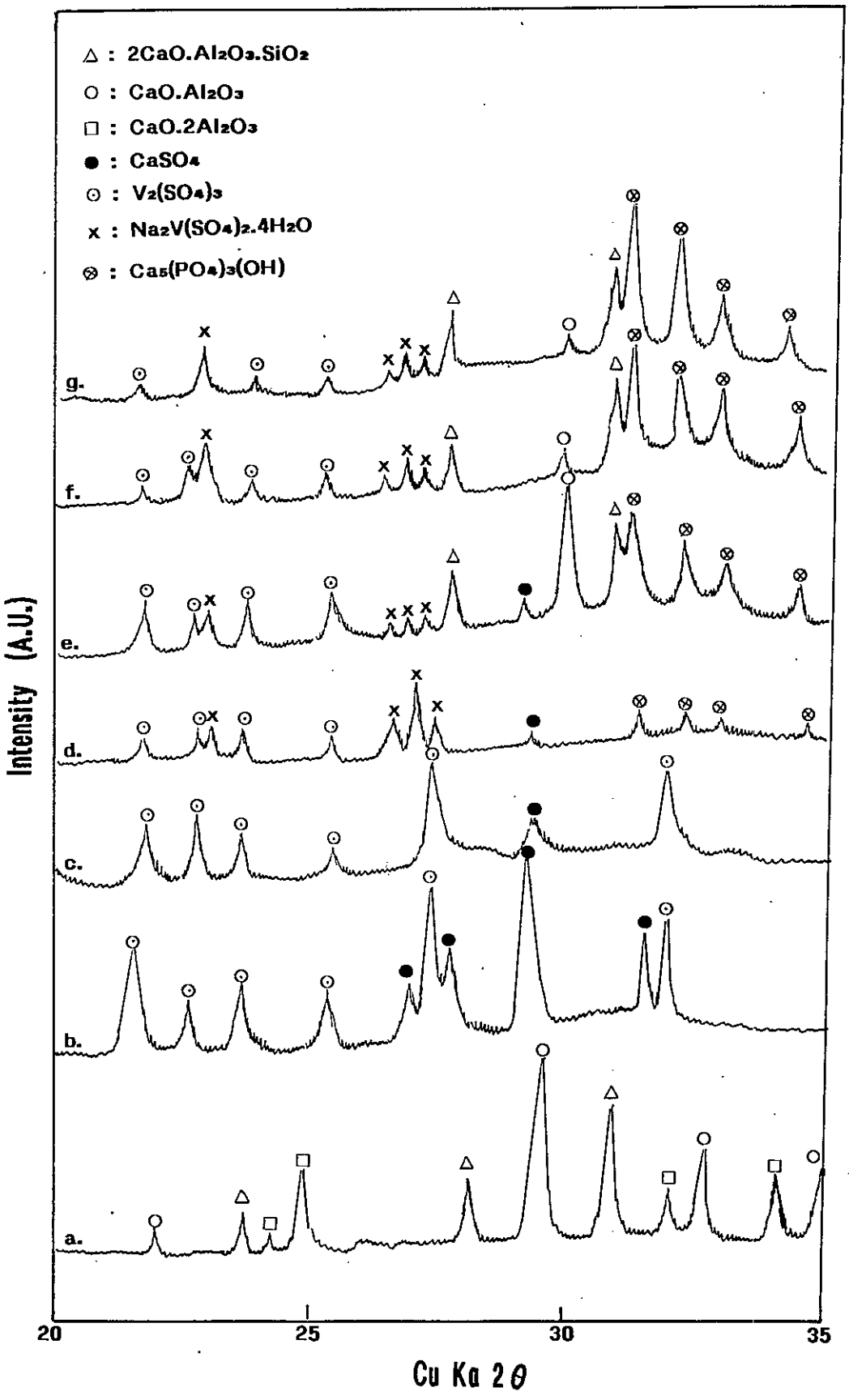

Figure 12. XRD patterns for (a) CAC additive, (b) raw BA powder, (c)28-day-air-cured BA-$NaPO_3$ cement system, (d) 80°C steam-cured BA-$NaPO_3$ system, (e) 28-day-air-cured BA-CAC-$NaPO_3$ cement system, (f) 28-day-water-cured BA-CAC-$NaPO_3$ system, and (g) 80°C-steam-cured BA-CAC-$NaPO_3$ system

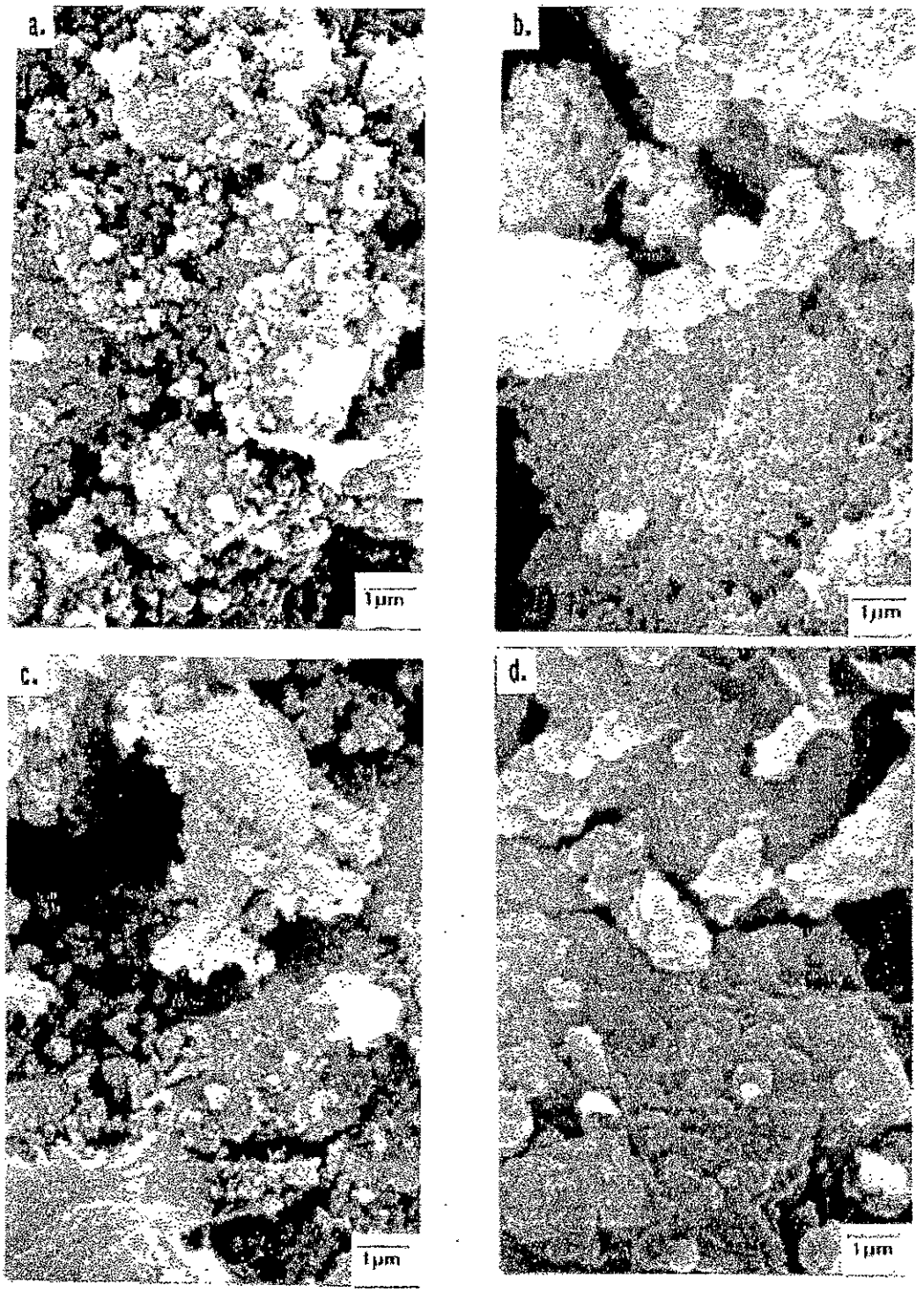

Figure 13. SEM images for (a) 28-day-air-cured BA-$NaPO_3$ system, (b) 80°C-steam-cured BA-$NaPO_3$ system, (c) 28-day-air-cured BA-CAC-$NaPO_3$ system, and (d) 28-day-water-cured BA-CAC-$NaPO_3$ system

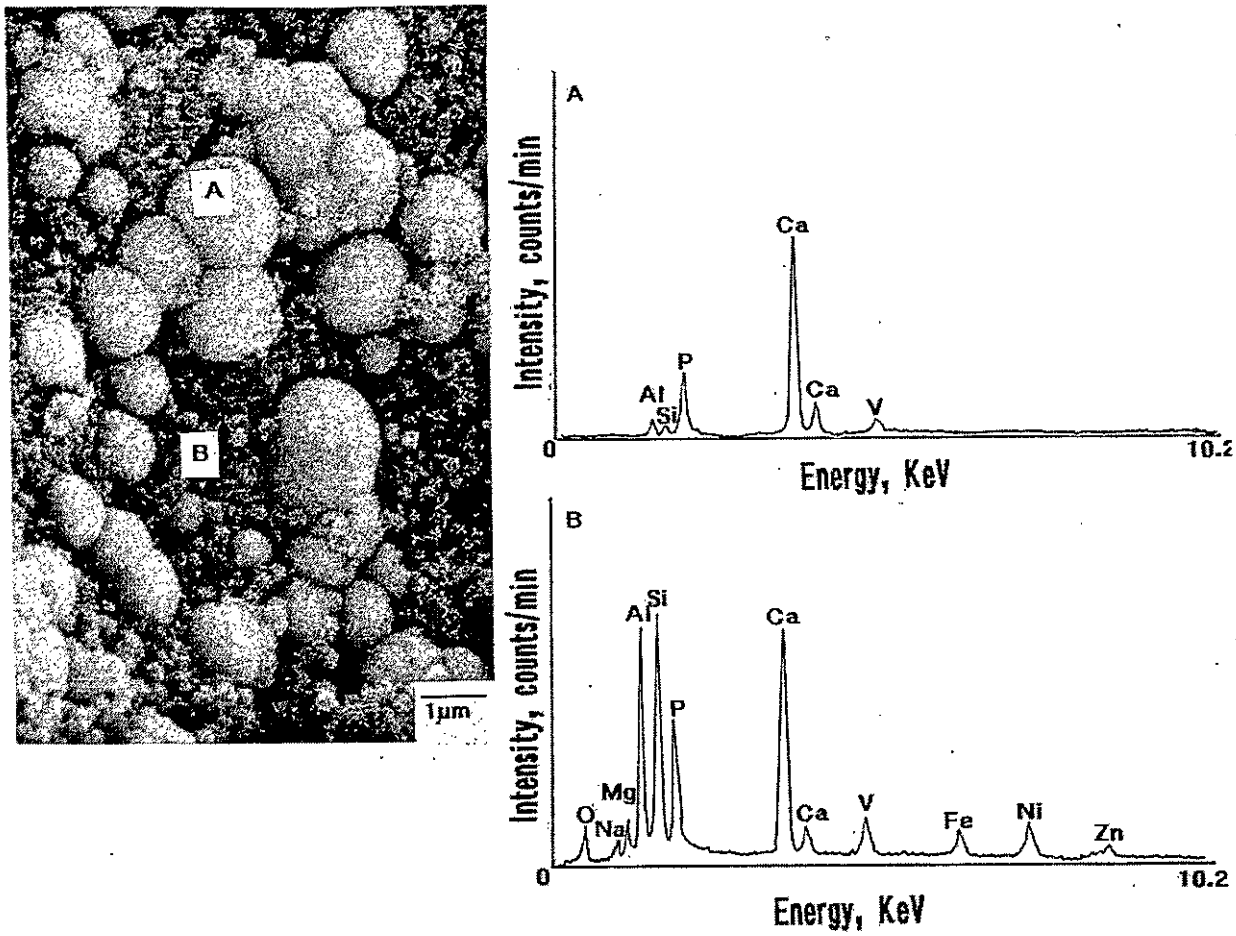

Figure 14. Well-crystallized calcium phosphate phase in 80°C-steam-cured BA-CAC-$NaPO_3$ cement system